THz Generation by GHz Multiplication in Superlattices

M. F. Pereira[a*], V. Anfertev[b], J. P. Zubelli[c] and V.Vaks[b]
[a] Department of Condensed Matter Theory, Institute of Physics, Academy of Sciences of the Czech Republic, Na Slovance 2, 182 21 Praha 8, Czech Republic
[b]Institute for Physics of Microstructures, RAS, Nizhny Novgorod, 603087, Russia
[c]IMPA, Rio de Janeiro, Brazil, 22460-320

Abstract. In this paper, we apply a hybrid Nonequilibrium Green's Functions and relaxation rate approximation approach to investigate frequency multiplication in the GHz to THz range delivering results in good agreement with experimental data for different input frequencies. A discussion of the current limitation of housing designs for the superlattices is given, based a simple model for the local electric field and in comparison with measured input powers delivered by a backward wave oscillator.

Keywords: Frequency Multiplication, GHz, THz, TERA-MIR, Nonlinearities, Semiconductor Superlattices

*Mauro F. Pereira**,** E-mail: pereira@fzu.cz

1 Introduction

The generation of high power coherent radiation in the GHz to THz ranges is a very important topic of recent research, recently fueled by findings that synchronization between superlattices leads to a dramatic increase in output power, with a potential to reach the THz range [1], or to be high power input sources for multipliers. Difference frequency generation via resonant optical nonlinearities pumped by a mid-infrared (MIR) quantum cascade laser QCL [2] is a promising approach for on-chip simultaneous emission from the MIR to the THz range but the range of interest here would require GHz resonances, which are difficult to achieve. At present, the key high compact solid-state sources that can be designed as oscillators [3] to deliver input radiation above 300 GHz for mixers and multipliers are Schottky diodes, Gunn devices and superlattice electron devices (SLEDs) [4], which are particularly high-performance fundamental sources in the 60–220GHz range [5]. InP Gunn devices, from which

second and third harmonics can also be extracted, have delivered 85μW at 480 GHz [6, 7]. This paper focuses on harmonic generation (or frequency multiplication). Before proceeding further, we should point out that wave mixing of different harmonics has been discussed in Ref. [8] and the idea of high frequency harmonic generation was developed in Refs. [9-11].

2 Outline of the mathematical model

When a SSL with period d, polarized by a voltage $E_{dc}\, d$, is excited by an electromagnetic field at frequency ν, $E_{ac}\cos(2\pi\nu t)$, the nonlinear current-voltage relation leads to harmonic current generation. For details of the derivation of the equations summarized next and used to deliver the numerical results of Section 3, see Ref. [7]. The harmonic currents in turn generate electromagnetic fields. The average power in the lth harmonic emitted by the superlattice is calculated from the Poynting vector, $\mathcal{P}_l(\nu) = \langle|\mathcal{J}_l(\nu)|^2\rangle\, T(\nu)$, where $T(\nu)$ is the waveguide transmission factor. The root-mean-square value $\langle|\mathcal{J}_l(\nu)|^2\rangle = (j_l^s)^2 + (j_l^c)^2$ stems from the lth components of the expansion of the nonlinear current in harmonics,

$$
\begin{aligned}
&j = j_{dc} + \textstyle\sum_{l=-\infty}^{\infty} j_l^c \cos(2\pi\nu t) + j_l^s \sin(2\pi\nu t),\\
&j_{dc} = \textstyle\sum_{p=-\infty}^{\infty} J_p^2(\alpha)\Upsilon(U),
\end{aligned}
\tag{1}
$$

$$
\begin{aligned}
&j_l^c = \textstyle\sum_{p=-\infty}^{\infty} J_p(\alpha)\left(J_{p+l}(\alpha) + J_{p-l}(\alpha)\right)\Upsilon(U),\\
&j_l^s = \textstyle\sum_{p=-\infty}^{\infty} J_p(\alpha)\left(J_{p+l}(\alpha) - J_{p-l}(\alpha)\right)\mathrm{K}(U),
\end{aligned}
$$

where J_p is the Bessel function of the first kind and order p, $\alpha = \frac{eE_{ac}d}{h\nu}$ and

$$
\Upsilon(U) = 2j_0\,\frac{U/\Gamma}{1+(U/\Gamma)^2},\ \mathrm{K}(U) = \frac{2j_0}{1+(U/\Gamma)^2}. \tag{2}
$$

It is a direct outcome of the theory that the total energy drop per period under irradiation is given by $U = E_{dc}d + phv$. This is fully consistent with measured current-voltage under irradiation [12-14]. The parameters j_0 and Γ are obtained by adjusting $j_{dc}$to the calculated current voltage (I-V) curve delivered by a microscopic Nonequilibrium Green's Functions (NEGF) approach. In ideal superlattices, the I-V would be perfectly asymmetric. However, imperfections distort the curve in actual structures. One of the fundamental reasons is the fact that the interface of GaAs over AlAs is worse than that of AlAs over GaAs. This effect has been included in the NEGF calculations of Ref. [7] and it is enough to explain why the flow of current from right to left cannot be equal from the value measured from left to right. The resulting I-V without illumination can be adjusted in excellent approximation by

$$j_0 = \begin{cases} j_0^-, & U < 0 \\ j_0^+, & U \geq 0 \end{cases}, \qquad \Gamma = \begin{cases} \Gamma^-, & U < 0 \\ \Gamma^+, & U \geq 0 \end{cases}. \tag{3}$$

This completes the model used in the simulations presented next in Section 3. At this point, we should point out that space-charge effects can lead to strong non-uniformities, far beyond the lack of symmetry due to different interfaces taken into account in this paper, which lead to $j_0^+ \neq j_0^-$ and $\Gamma^+ \neq \Gamma^-$. Full consideration of this highly nonlinear and to the best of our knowledge unstudied phenomena, are beyond the scope of this paper and will be the subject of future investigation.

2 Numerical results and discussions

The SSL structure used has 18 periods of 6.23 nm each with 18 monolayers GaAs and four monolayers AlAs. It was homogeneously doped with silicon and an electron density of 1.5×10^{18} cm^{-3} has been used in the NEGF calculations [7, 15, 16]. Experiments have been

performed at room temperature and T=300K has been used in the calculations. The SSL was placed in a waveguide chamber and the waveguide transmission factor $T(\nu)$, calculated with MICROWAVE OFFICE [17], is shown in the inset of Fig. 1. This blocks the input radiation from the backward wave oscillator (BWO) pumps at 130, 141, 150 and 160 GHz from the output. The SSL harmonic power was measured with a Fourier transform spectrometer and the receiver was a silicon He-cooled bolometer. Details of the experimental setup, equipment used and signal to noise ratios are given in Ref. [7]. The experimental setup imposes a number of geometric factors that ultimately limit the harmonic power detected and at this point, these factors cannot be introduced realistically in the simulations. They are however, the same for each harmonic and thus the meaningful way to compare theory and experiments is to eliminate the unknown factors by taking the ratios to a reference harmonic power, chosen here as the strongest measured, i.e. the third harmonic. Thus for both experiments (symbols) and calculations (solid lines) the Normalized Harmonic Power shown in Fig. 1 is $NHP_l(\nu) = \mathcal{P}_l(\nu)/\mathcal{P}_3(\nu)$. The parameters extracted from NEGF calculations and used in Eq. (3) are the same as in Ref. [7]. i.e Γ^-, Γ^+= 20, 21 meV and j_0^-, j_0^+= 1.94 , 2.14 × 10^9 A/m^2.

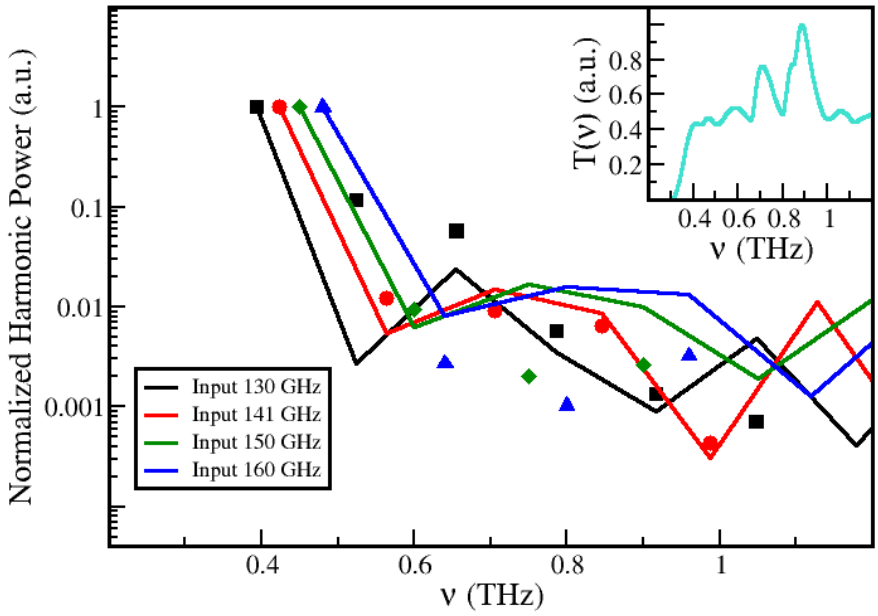

Fig. 1. Normalized Harmonic Power $NHP_l(\nu) = \mathcal{P}_l(\nu)/\mathcal{P}_3(\nu)$ of the 1[th] harmonic to the 3[rd] harmonic nonlinearly generated by input fields oscillating respectively at 130, 141, 150 and 160 GHz for the black square, red circle, green diamond and blue triangle curves. The corresponding solid lines have been calculated using our theory and assuming incident field powers characterized by α=35.2, 28.3, 26.1 and 23.7. See Table 1. The inset shows the normalised transmission function of the waveguide structure where the superlattice is inserted.

The present experimental setup does not allow to determine which fraction of the input power from the BWO actually reaches the superlattice. A nonlinear least-squares curve-fitting algorithm based on the Levenberg-Marquardt method [18] has thus been used to determine α. In order to estimate what is the input field power inside the superlattice, based on the value found for α, we assume that the field delivered by the BWO at the SSL is a plane wave of amplitude E_{ac}, and frequency ν (in GHz) a vaccum impedance of $Z_0 = 377$ a spot size given

by the surface of the SSL exposed to the field, $A = 112$ nm $\times$ 2 μm and the SSL period $d =$ 6.23 nm. The connection between input power (in mW) and $\alpha = \frac{eE_{ac}d}{h\nu}$ is given by

$$P_{in}(mW) = 2.941 \times 10^{-9}\, \nu^2 \alpha^2. \quad (4)$$

Table 1 gives numerical values for the difference frequencies investigated.

Table 1. Connection between the power delivered by the BWO at frequency ν, BWO (mW) and the estimated value of the power that actually reaches the SSL, Pin (μW), using Eq. (4) based on the value found for α.

ν (GHz)	BWO (mW)	α	P_{in} (μW)
130	1.8	35.2	61.6
141	4.1	28.3	47.0
150	11.2	26.1	45.2
160	33.9	23.7	42.2

It is clear from the results that the theory developed in Ref. [7] is valid for different input frequencies and that the experimental setup must be improved to prevent higher frequency inputs to be blocked. Note that the whole coupling setup requires a factor of 18.3 more power if the input frequency is increased from 130 to 160 GHz. Once these limitations are solved SSL multipliers, integrated e.g with SLEDs can become the prime source for the GHz-THz, complementing the dominating role the QCLs have in the Mid Infrared and delivering coherent power to extend polaritonic effects to the GHz range [19, 20]. Note that THz QCLs can already deliver over 1 W of output power [21]. However, intrinsic limitations will most likely always require cryo-cooling, even if lasing without inversion effects concepts can make the operating temperatures a bit higher [22-24] and thus different room temperature concepts, such as the one discussed in this paper are of definite relevance in the development of practical THz sources.

4 Conclusion

In summary, the hybrid NEGF–relaxation rate approximation method for GHz to THz multiplication based on nonlinearities in the nonlinear response of the current-voltage relation of semiconductor superlattices has been investigated for different frequencies. The good qualitative agreement with experiments further support applications of the method to the simulation of new frequency multiplication devices and further understanding of the related microscopic phenomena. It shows a strong need for novel designs allowing a larger frequency range to be multiplied in each housing waveguide and coupling architecture. We hope that this paper can be a stimulus for strong progress in the field, not ably in a frequency range where quantum cascade lasers cannot efficiently operate.

Appendix A: Determining Numerical Parameters from Experiments

In the main part of the text, we have highlighted the fact that the present experimental setup does not allow to determine which fraction of the input power from the BWO actually reaches the superlattice to calculate the parameter α. This requires a careful analysis of the problem which we shall now describe.

As usual, one proceeds by introducing an algorithm to compute the value of the measured results by making use of analytical and numerical procedures, and then computes the difference between the predicted computational results and the experimental ones. Such difference is measured in an appropriate norm of a large dimensional weighted Euclidean space. The use of appropriate weights avoids the information loss due to the different scales involved. The procedure of computing the would-be measurements for a given set of parameters is the so-called parameter-to-solution map. In an ideal situation where the model would describe perfectly the phenomena and in the absence of noise, or numerical errors, the

minimum of the distance between the parameter-to-solution map evaluated at the precise parameters for the problem and the data would be zero. However, this is not the case in practical situations and one resorts to the minimization of the distance between the data and the parameter-to-solution map. In our case the latter map is far from a linear one and thus after the computation of the distance between the predicted data and the measurements leads to a rather difficult minimization problem. Indeed, the problem under consideration is not a convex one and thus does not possess a global minimum. We thus performed our analysis first by approximating the minimum through a simulated annealing approach and then zeroed into the actual minimum by the Levenberg-Marquadt algorithm. We recall that simulated annealing algorithms are based on a meta heuristic to approximate the global minimum in a large search space whereby one mimics the annealing procedure from metallurgy that finds the minimal energy of a thermodynamical system [25]. We have calculated the parameters j_0^-, j_0^+, $\Gamma^-$and Γ^+per direct comparison between the current without illumination calculated with NEGF techniques and Eq. (3) as explained in Ref. [7].

A possible solution to make the method more accessible to experimentalists that have no access to advanced NEGF techniques is to consider not only α, but the full ensemble $\{\alpha, j_0^-, j_0^+, \Gamma^-\text{and } \Gamma^+\}$ as unknowns. In such more complex situation, once again the presence of local minima requires the usage of two-step procedure, whereby one first locates the general region of the global minimum by means of the simulated annealing technique and then refines the solution with a more precise method (such as for example Levenberg-Marquadt).

Acknowledgments

The authors thank A. Wacker, D. Winge and A.S. Rodrigues and acknowledge support from COST ACTION MP1401.

References

1. M.B. Gaifullin, N.V. Alexeeva, A.E. Hramov, V.V. Makarov, V.A. Maksimenko, A.A. Koronovskii, M.T. Greenaway, T.M. Fromhold, A. Patané, A. C.J. Mellor, C. J. and F.V. Kusmartsev, and A.G. Balanov, Microwave Generation in Synchronized Semiconductor Superlattices, Phys. Rev. Applied 7, 044024 (2017).
2. M. Razeghi, Q. Y. Lu, N. Bandyopadhyay, W. Zhou, D. Heydari, Y. Bai, and S. Slivken, Quantum cascade lasers: from tool to product, Opt. Express 23, 8462 (2015).
3. H. Eisele, State of the art and future of electronic sources at terahertz frequencies, Electron. Lett. 46, 8 (2010).
4. H. Eisele, S. P. Khanna, and E. H. Linfield, Superlattice electronic devices as high-performance oscillators between 60-220 GHz, Appl. Phys. Lett. 96, 072101 (2010).
5. H. Eisele, 480GHz oscillator with an InP Gunn device, Electron. Lett. 46, 422 (2010).
6. H. Eisele, Third-Harmonic Power Extraction from InP Gunn Devices up to 455 GHz, IEEE Microw. Compon. Lett. 19, 416 (2009).
7. M.F. Pereira, D. Winge and A. Wacker, J.P. Zubelli, A.S. Rodrigues, V. Anfertev and V. Vaks, "Theory and Measurements of Harmonic Generation in Semiconductor Superlattices with Applications in the 100 GHz to 1 THz Range", Phys. Rev. B 96, 045306 (2017).
8. K.N. Alekseev, M.V. Erementchouk and F.V. Kusmartsev, Direct-current generation due to wave mixing in semiconductors, Europhys. Lett. 47, 595 (1999).

9. K.N. Alekseev, E.H. Cannon, F.V. Kusmartsev and D.K. Campbell, Fractional and unquantized dc voltage generation in THz-driven semiconductor superlattices, Europhys. Lett. 56, 842 (2001)
10. K.N. Alekseev and F. Kusmartsev, Pendulum Limit, Chaos and Phase-Locking in the Dynamics of Ac-Driven Semiconductor Superlattices, Physics Letters A 305, 281 (2002).
11. N. Alexeeva, M.T. Greenaway, A.G. Balanov, O. Makarovsky, A. Patanè, M.B. Gaifullin, F. Kusmartsev and T. M. Fromhold, Controlling High-Frequency Collective Electron Dynamics via Single-Particle Complexity, Phys. Rev. Lett. 109, 024102 (2012).
12. P. S. S. Guimaraes, B. J. Keay, Jann P. Kaminski, S. J. Allen, Jr., P. F. Hopkins, A. C. Gossard, L. T. Florez, and J. P. Harbison, Photon Mediated Sequential Tunneling in Intense Terahertz Fields, Phys. Rev. Lett. 70, 3792 (1993).
13. B. J. Keay, S. J. Allen Jr., J. Galan, J. P. Kaminski, K. L. Campman, A. C. Gossard, U. Bhattacharya, and M. J. M. Rodwell, Photon-Assisted Electric Field Domains and Multiphoton-Assisted Tunneling in Semiconductor Superlattices, Phys. Rev. Lett. 75, 4098 (1995).
14. A. Wacker, A.-P. Jauho, S. Zeuner, and S. J. Allen, Sequential tunneling in doped superlattices: Fingerprints of impurity bands and photon-assisted tunneling, Phys. Rev. B 56, 13268 (1997).
15. T. Schmielau and M. F. Pereira, Jr., Nonequilibrium many body theory for quantum transport in terahertz quantum cascade lasers, Appl. Phys. Lett. 95, 231111 (2009).
16. D. O. Winge, M. Franckie, C. Verdozzi, A. Wacker, and Mauro F. Pereira, Simple electron-electron scattering in non-equilibrium Green's function simulations, J. Phys.: Conf. Ser. 696, 012013 (2016).
17. MICROWAVE OFFICE: http://www.awrcorp.com/products/ni-awrdesign-environment/microwave-office
18. J. J. Moré, The Levenberg-Marquardt algorithm: Implementation and theory, in Numerical Analysis, edited by G. A. Watson, LectureNotes in Mathematics, Vol. 630 (Springer-Verlag, Berlin, 1977, pp. 105–116.

19. M.F. Pereira, TERA-MIR Radiation: Materials, Generation, Detection And Applications II, Opt Quant Electron 47, 815-820 (2015).
20. M.F. Pereira, IA Faragai, Coupling of THz radiation with intervalence band transitions in microcavities, Optics express 22 (3), 3439-3446 (2014).
21. L. Li, L. Chen, J. Zhu, J. Freeman, P. Dean, A. Valavanis, A.G. Davies and E.H. Linfield, Terahertz quantum cascade lasers with >1 W output powers, Electron. Lett. 50, 309 (2014).
22. M. F. Pereira and S. Tomić, Intersubband gain without global inversion through dilute nitride band engineering, Appl. Phys. Lett. 98, 061101 (2011).
23. M.F. Pereira Jr., Intervalence transverse-electric mode terahertz lasing without population inversion, Phys. Rev. B78, 245305 (2008).
24. M.F. Pereira, The Linewidth Enhancement Factor of Intersubband Lasers: From a Two-Level Limit to Gain without Inversion Conditions, Applied Physics Letters 109, 222102 (2016).
25. W.H. Press, S.A. Teukolsky, W.T. Vetterling and B.P. Flannery, "Section 10.12. Simulated Annealing Methods". Numerical Recipes: The Art of Scientific Computing (3rd ed.). New York: Cambridge University Press. ISBN 978-0-521-88068-8) (2007).

Biographies

Mauro Fernandes Pereira is a Professor and Head of Department of Theory of Condensed Matter, Institute of Physics, Academy of Sciences of Czech Republic. His main research interest is on nonequilibrium manybody theory applied to quantum and nonlinear optics and transport in semiconductor materials and has co-authored over 120 publications. He received his PhD at the Optical Sciences Center, University of Arizona and is a Fellow of SPIE.

Jorge P. Zubelli obtained his PhD from the University of California at Berkeley (USA) in 1989. He is Professor of Mathematics at the National Institute for Pure and Applied Mathematics (IMPA), Rio de Janeiro, Brazil, and heads the Laboratory for Mathematical Modeling and Analysis in the Applied Sciences (LAMCA) at IMPA. He works on Mathematical Modeling and Inverse Problems and co-authored over 80 research and technical contributions.

Vladimir A. Anfertev received his PhD from the Faculty of Radiophysics in Lobachevsky State University, Nizhny Novgorod, Russia in 2016. His research interests are use of quantum superlattice electronics and quantum cascade lasers for THz non-stationary spectroscopy.

Vladimir L. Vaks received his PhD from the Faculty of Radiophysics in Lobachevsky State University 1970 and a Dr. Sci. degree in 2003. He is currently Head of Terahertz Spectrometry Department of Institute for Physics of Microstructures Russian Academy of Sciences (Nizhny Novgorod, Russia) and lecturer in Lobachevsky State University. His expertise includes the development of the high resolution THz spectroscopy methods and their application in medicine, hi-tech and security systems. Vladimir Vaks has co-authored over 240 papers.

Caption List

Fig. 1 Normalized Harmonic Power $NHP_l(\nu) = \mathcal{P}_l(\nu)/\mathcal{P}_3(\nu)$ of the l^{th} harmonic to the 3^{rd} harmonic nonlinearly generated by input fields oscillating respectively at 130, 141, 150 and 160 GHz for the black square, red circle, green diamond and and blue triangle curves. The

corresponding solid lines have been calculated using our theory and assuming incident field powers characterized by α=35.2, 28.3, 26.1 and 23.7. See Table 1. The inset shows the normalised transmission function of the waveguide structure where the superlattice is inserted.